Simulation of Viscous Flows with a Gridless Particle Method

FOTIOS G. STAMATELOS and JOHN S. ANAGNOSTOPOULOS
School of Mechanical Engineering / Fluids Section
National Technical University of Athens
9, Iroon Polytechniou ave., Zografou, 15780 Athens
GREECE
sfotis@fluid.mech.ntua.gr j.anagno@fluid.mech.ntua.gr

Abstract: The aim of this paper is to present the numerical simulation of the evolution of the viscous, low Reynolds flows in two-dimensional cases with the use of the Smoothed Particle Hydrodynamics (SPH) method. This work is considered as the first step towards the simulation of complex three-dimensional flows, which occur in impulse water turbines. The method was originally developed for solving problems of astrophysical nature and belongs to the meshless methods, as it does not require any computational grid. A set of descrete fluid particles is used to represent the continuous fluid, and their trajectories are being calculated in a Lagrangian sense through time. The 2-D test cases examined in this paper are the Couette and the Poiseuille Flow, and the basic problem of the liquid column collapse (Dam Break). For the first two test cases the numerical results were tested against analytical solutions from the literature, while for the third test case experimental measurements were used for the validation of the calculations. The agreement of the numerical results with the corresponding analytical and experimental data is quite good and encouraging towards the use of the SPH method in modelling of more complex, unsteady and multiphase flow fields, while the performance of the algorithm referring to the speed of the calculations and the qualitative results is remarkable.

Key-Words: - Smoothed Particle Hydrodynamics (SPH), Dam Break, Couette and Poiseuille Flow, Numerical Modelling

1 Introduction

Initially the SPH method was expressed by Lucy [1] and then used in astrophysical problems, such as the movement of the stars and the asteroids by Gingold and Monaghan [2], while later it was applied for problems of continuum solid and fluid mechanics. Monaghan in [3] presents an extended review on the SPH method. The method was initially developed for compressible flows and then it was extended to be applied in free surface flows [4], [5] through an artificial fluid which can be considered slightly compressible. Such an assumption was necessary in order to overcome the problem of large sonic velocities and allowed the use of larger computational time step.

The SPH method is characterised as a mesh-free particle method since it does not involve any mesh during the calculation procedure and its aim is only to track the trajectories of the particles that represent the moving fluid [3]. The mesh-free nature of the method allows overcoming problems such as the generation of the grid, which sometimes can be very time consuming, or the simulation of the flow field near complex boundary geometries or even the simulation of free surface flows, as no special conditions are required at the interface. It also gives the opportunity to model flows with moving or deforming boundaries or simulate the interaction of several fluid phases [6]. Apart from the above the main advantages of the SPH method are that pure advection can be treated accurately and that when more than one materials are involved in the calculations then the interface problems may be solved easily. Moreover the resolution of the problem can be made easily adapted to the location and to the time while due to the close similarity between SPH and molecular dynamics it is permitted to include complex physics as well [3]. It should also be noted that the SPH is quickly approaching its mature stage, which means that it can be applied for micro-scale to macro-scale problems and from discrete to continuum systems. Some of the fields that the SPH method is already been applied are the modelling of

the casting process [7] or the simulation of interfacial flows [8]. It is also applied for the simulation of viscous flows [9] and water waves as well [5] and [10]. However, the numerical errors of SPH can be larger than those of grid-based methods, and also it can be more computational expensive for a given application [6].

The aim of this work is to develop and evaluate a numerical algorithm based on the SPH method, as a first step towards the modelling of the complex, unsteady flow in impulse water turbines. The results are compared with experimental and analytical data from the literature with encouraging agreement.

2 The SPH Method

2.1 Theoretical Background

The SPH method uses the Lagrangian concept. Most commercial codes for simulating fluid dynamics problems are based on the continuous Eulerian method. The disadvantages, which arise during such a simulation, may sometimes not be negligible. The most important of them is that when using a fixed mesh the time history of the flow variables at a fixed point of the fluid cannot be tracked as these variables are being calculated according to the cells. Irregular or complicated geometries are also difficult and extremely time consuming in order to be represented when using a fixed mesh method. The accurate determination of the position of free surfaces, deforming boundaries or even material interfaces is very difficult to achieve in the Eulerian method. Finally in many cases the resolution of the domain discretization- and hence the accuracy of the results- has to be sacrificed because the use of a more coarse grid is necessary. Such problems could be overcome if a gridless method, which follows the trajectories of fluid particles, is applied.

According to the theory of the SPH method, the fluid is represented by a set of particles, which follow the movement of the fluid. These particles carry all the physical quantities of the fluid, such as its density, velocity and pressure. Depending on the problem, the particles may also carry the local energy of the fluid.

One of the main features of the SPH method is its adaptive nature, which enables it not to be affected by the arbitrariness of the particles distribution. This leads to the advantage of handling situations of large deformations. The SPH approximation does not require any pre-defined mesh to provide any connective of the particles in the process of computation and it works well enough even without any particle refinement procedure [6]. The representative particles are free to move in the computational domain and since they carry all the fluid properties they form the computational frame for solving the partial differential equations, which describe the conservation laws of the continuum fluid dynamics.

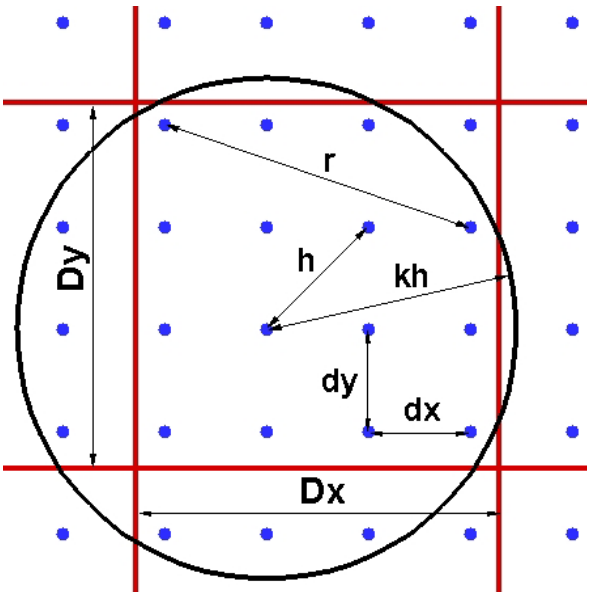

Figure 1. Geometric characteristics of the grid and the initial distribution of the particles.

The equations governing the movement and the properties of the fluid particles are expressed as summation interpolants using a kernel function W. Theoretically, the calculation of the properties of a particle α requires knowledge of the interaction between the particle α and the rest of the particles in the flow field. In practice though, a procedure like this would be extremely time consuming so each particle is affected only from those particles that are within a certain distance from it, which is the smoothing length h.

If A is a property function of the fluid then the value of A_α for the particle α will be:

$$A_a = \int A_b W_{ab} d\vec{r}_{ab} \qquad (1)$$

where A_b is the value of the function A for the neighbor particle b, W_{ab} is the value of the kernel function and $\vec{r}_{ab}$ is the distance between particles α and b. So in SPH formulation Eq. (1) becomes:

$$A_a = \sum_b m_b \frac{A_b}{\rho_b} W_{ab} \tag{2}$$

From the above equation the calculation of the first derivative can be expressed as follows:

$$\nabla A_a = \sum_b m_b \frac{A_{ab}}{\rho_a} \nabla W_{ab} \tag{3}$$

where $A_{ab}=A_a-A_b$.

In order to numerically simulate a flow field using the SPH method there are 4 basic steps. First of all the problem domain where the partial differential equations are defined must be discretized. Then a certain method must be applied in order to provide an approximation of the values of the field functions and their derivatives, followed by the function approximation, which is applied to the partial differential equations in order to produce a set of ordinary differential equations in a discretized form with respect only to time. Finally, the set of ordinary differential equations is solved using a numerical integration scheme.

2.2 The Kernel Function

There are several expressions of the kernel function which can be applied for the calculations of the properties of the fluid particles. For the simulation of the movement of spherical stars Gingold and Monaghan [2] used a Gaussian kernel, while at the same time Lucy [1] used a bell-shaped function. Monaghan and Lattanzio [11] introduced a kernel based on the B-spline function and Morris [12] applied higher order splines, which proved to be more stable than the previous expressions.

The kernel function, apart from being spatially differentiable, must satisfy some other conditions as well, as the positivity in order to avoid unacceptable results such as negative density or energy, and the monotonicity, according to which the influence that one particle exerts to the other must be monotonically decreasing with the increase of their distance. Moreover, it must be even, so that particles from the same distance but opposite sides should have the same influence on a given particle, smooth, in order to produce more accurate results, and finally satisfy the Dirac delta function condition:

$$\lim_{h\to 0} W_{ab} = \delta \tag{4}$$

The kernel function used in this work is the one originally proposed by Violeau, [13]:

$$W(q) = \frac{a_d}{h^d} \begin{cases} \left(\frac{5}{2}-q\right)^4 - 5\left(\frac{3}{2}-q\right)^4 + 10\left(\frac{1}{2}-q\right)^4 & 0 \le q \le 0.5 \\ \left(\frac{5}{2}-q\right)^4 - 5\left(\frac{3}{2}-q\right)^4 & 0.5 \le q \le 1.5 \\ \left(\frac{5}{2}-q\right)^4 & 1.5 \le q \le 2.5 \\ 0 & q \le 2.5 \end{cases} \tag{5}$$

where h is the smoothing length, and q is the ratio $|r_{ab}|/h$. The term α_d is equal to $(96\pi/1199)$ for 2D problems and $(\pi/20)$ when the problem expands in the 3D space. The general behavior of the kernel function is shown in Figure 2., [13].

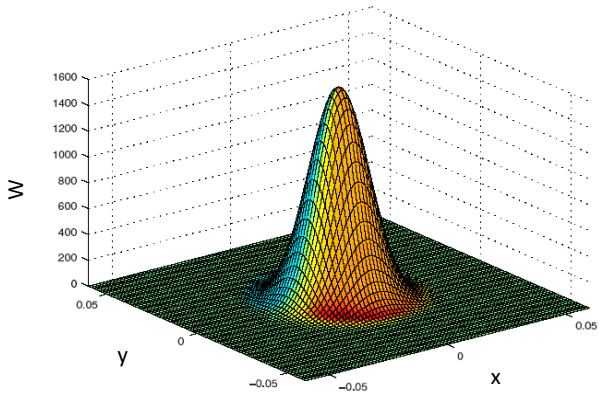

Figure 2. Kernel Function behavior in the 2D space.

2.3 Equations of Motion

The fluid flow simulation is based on the continuity and momentum Navier-Stokes equations:

Continuity: $$\frac{d\rho}{dt} = -\rho \nabla \cdot \vec{u} \tag{6}$$

Momentum: $$\frac{d\vec{u}}{dt} = -\frac{1}{\rho}\nabla p + \nu\nabla^2\vec{u} + \vec{g} \quad (7)$$

where ρ is the density, p the pressure, ν the kinematic viscosity and g the gravity acceleration. According to the SPH method, Eqs. (6) and (7) can be written for a 2D field as follows:

Continuity:
$$\frac{d\rho_a}{dt} = \sum_b m_b \left[\left(u_b - u_a\right)\frac{\partial W}{\partial x} + \left(v_b - v_a\right)\frac{\partial W}{\partial y} \right] \quad (8)$$

Momentum:
$$\left.\begin{aligned} \frac{du_a}{dt} &= -\sum_b m_b \left[\left(\frac{p_a}{\rho_a^2} + \frac{p_b}{\rho_b^2} \right)\frac{\partial W}{\partial x} - \Pi_{ab} \right] + g_x \\ \frac{dv_a}{dt} &= -\sum_b m_b \left[\left(\frac{p_a}{\rho_a^2} + \frac{p_b}{\rho_b^2} \right)\frac{\partial W}{\partial y} - \Pi_{ab} \right] + g_y \end{aligned}\right\} \quad (9)$$

where the term Π_{ab} contains the viscous forces. Various expressions have been proposed for this term [14], [7], [15] and here we use the one of Monaghan [3]:

$$\Pi_{ab} = -16\frac{\mu_a\mu_b}{\rho_a\rho_b\left(\mu_a + \mu_b\right)}\left(\frac{\vec{v}_{ab}\cdot\vec{r}_{ab}}{\vec{r}_{ab}^{\,2}}\right)\nabla W_{ab} \quad (10)$$

2.4 Equation of State

As mentioned before the fluid particles carry with them all the properties of the fluid itself. The fluid pressure calculation is a critical point of the SPH method, and due to the lack of an adequate analytical expression, it is usually estimated through an equation of state, as first suggested by Monaghan [4]:

$$p_a = \frac{\rho_0 c_0^2}{\gamma}\left[\left(\frac{\rho_a}{\rho_0} \right)^{\gamma} - 1 \right] \quad (11)$$

in which ρ_0 is a reference density, c_0 the local speed of sound and γ=7 for water. Eq. (11) may be applied for weakly incompressible fluids as it can simulate incompressibility with sufficient accuracy. However, for numerical reasons, the speed of sound is set to an artificial value, and not its physical one, which is usually taken 10 times of the maximum flow speed, keeping this way the density fluctuations below 1%. Adopting such an approximation for the pressure the SPH method appears to be a weakly compressible one. Solving a pressure Poisson equation is sometimes preferred because of the possible instabilities that Eq. (11) may add to the calculations. The good balance between accuracy and simplicity for SPH making use of Eq. (11) is the feature that makes it so commonly used.

2.5 Solid Boundaries Treatment

Three main ways of treatment have been used for the solid boundaries of the flow field. Their influence may be modelled by using repulsive forces to assure the particle non-penetration condition, which usually have the Lennard-Jones form [4].

$$f\left(r\right) = D\left[\left(\frac{r_0}{r} \right)^{p_1} - \left(\frac{r_0}{r} \right)^{p_2} \right]\frac{\vec{r}}{r^2} \quad (12)$$

As the fluid particles move closer to the wall the L-J forces evolve and decelerate them leading to the appropriate non-penetration condition, Fig. 3(a). This way of boundary treatment is necessary for the cases where the fluid particles tend to move towards the wall surface, and their velocity is not exactly parallel to the boundary.

A second technique uses 'ghost' or 'mirror' particles to represent the solid wall. The wall surface is considered locally as a symmetry plane in order to create and locate the 'mirror' particle of an approaching fluid particle [14], [16], Fig. 3(b). The 'mirror' particles have the same properties with their corresponding fluid ones but opposite normal velocities, to prevent particle penetration.

The third method to represent the walls is through the use of a number of 'fixed' particles, the properties of which remain constant in time except from their density [13], Fig. 3(c). The latter increases as the fluid particles get closer to the wall thus leading to a pressure increase of the wall particles and finally decreasing the fluid particles velocity near this region securing again the non-penetration. The formation of the ways of treating the boundaries is shown in Fig. 3.

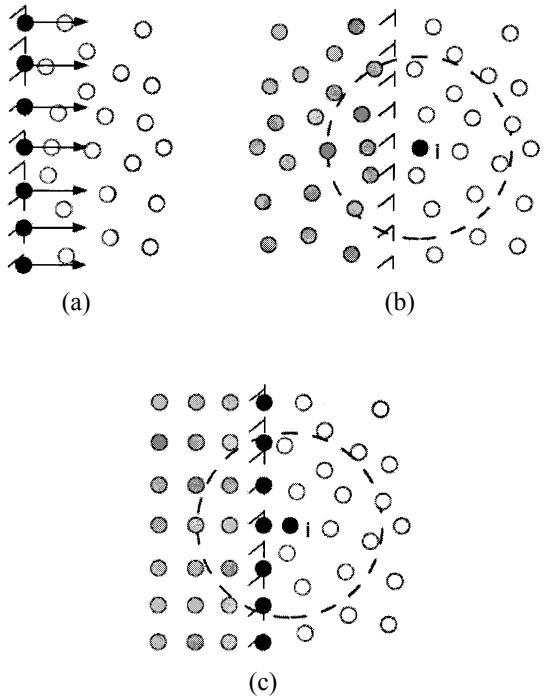

Figure 3. Solid Boundaries Treatment: (a) L-J Forces, (b) 'Ghost-Mirror' Particles and (c) 'Fixed' Particles

2.6 Computational details

The accuracy of the numerical results depends on the number of representative fluid particles which are tracked. The latter may also depend on the specific flow conditions (e.g. geometry, Re), and must be determined for each examined case.

The particle equations are integrated in time usually with a predictor-corrector scheme or other high-order numerical methods (e.g. Runge-Kutta), using constant or adaptive time-step. The maximum permissible step for stability is obtained by Courant type criteria [14].

In order to produce an algorithm, which can be used in various test cases, two independency studies were conducted. The first one had to do with the number of representative particles for the fluid and the second one with the time step of the integration. Results for both these studies will be presented below.

Despite the fact that SPH is a gridless method, a so-called "background" grid was adopted. This grid helped towards the calculation of the time and space averaged values of the velocities, density and pressure. At each time step the average value of these properties is being calculated for each grid cell from the particles that are within its limits. After the steady state of the flow is reached the space average values are stored for several time steps in order to finally compute the time-average values. With this approximation the algorithm allows the contour plotting of the fluid properties at the steady state flow field conditions. Figure 4 exhibits the initial distribution of the particles in a 2-D Couette flow between two parallel plates.

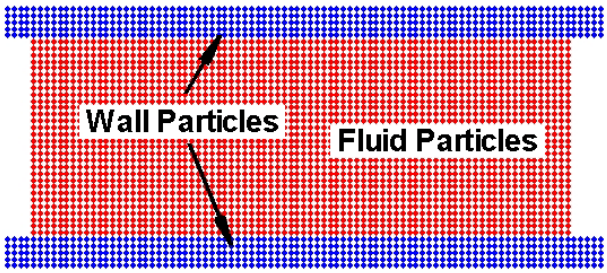

Figure 4. Initial particles distribution for the 2-D Couette flow.

3 Evaluation of the Model

3.1 Couette Flow

The first test case is the modelling of the 2D Couette flow between two infinite plates located at $y=-L/2$ and $y=+L/2$, respectively (Fig. 5).

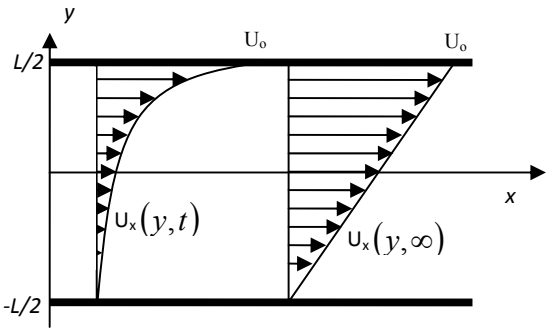

Figure 5. Couette Flow.

At the beginning of the simulation the system is at rest and at time $t=0$ the upper plate starts to move with a constant horizontal velocity U_o. The flow finally reaches the steady state, with a linear velocity profile (Fig. 5).

The transient behaviour of this flow can be obtained by the following analytical expression [14]:

$$u_x(y,t) = U_0 \frac{y}{L} + \sum_{n=1}^{\infty} \frac{2U_0}{n\pi}(-1)^n \sin\left(n\pi \frac{y}{L}\right) \exp\left(-\nu \frac{n^2\pi^2}{L^2} t\right) \quad (13)$$

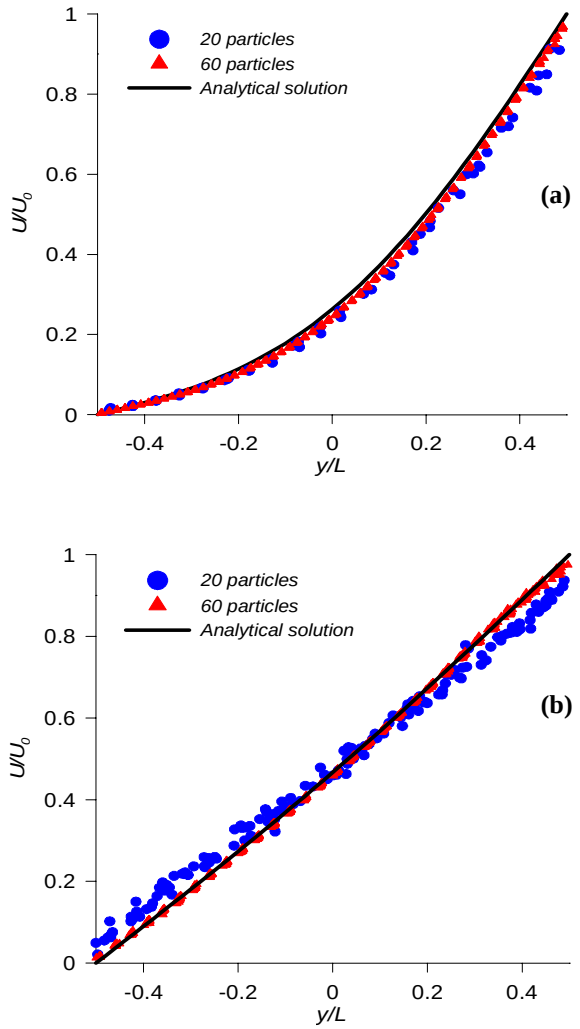

Figure 6. Comparison of the results with different particles number, at: (a) t=0.1 sec and (b) t=0.3 sec.

A numerical study is conducted at first in order to find the number of representative fluid particles that produce independent results for the average flow field. The calculations were made for Reynolds number equal to 50 (defined as $Re=U_oL/\nu$), and five different cases were simulated using initial particle distances of $L/20$, $L/30$, $L/40$, $L/50$ and $L/60$, respectively.

The axial velocity profiles of the particles for two of the above cases are compared with the analytical solution in Fig. 6 at two time instants, one during the transient period (t = 0.1 sec), Fig. 6a, and the second when approaching the steady state (t = 0.3 sec), Fig. 6b. The use of 20 particles across the plates produces more scattered results, which deviate from the analytical solution (Fig. 6b), whereas for the 60 particles case the results precision is clearly enhanced and the agreement with theory is very good. It was found that the results become practically identical when more than 40 particles are used, as it is showed in Fig. 7, therefore the *L/50* arrangement is selected for all the rest numerical experiments.

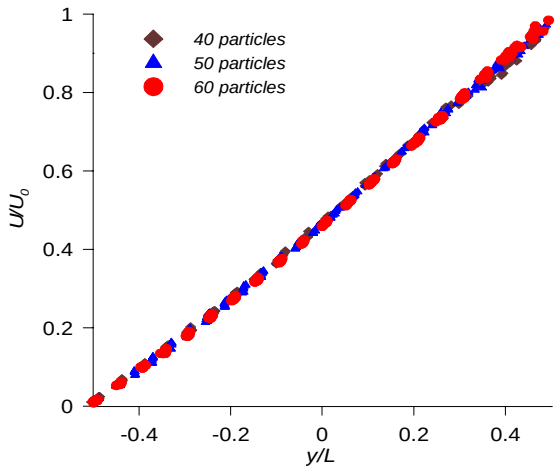

Figure 7. Results comparison for $L/40$, $L/50$ and $L/60$ distance between the fluid particles, at t=0.3 sec.

Apart from the particles' independency, a time step independency study was also conducted for the same test case. A small time step, $dt=6.25\text{x}10^{-4}$ sec, was found to be necessary in order to avoid instabilities of the numerical integration scheme. The simulation of the flow using $dt/2$ and $dt/4$ values gave exactly the same results, therefore no smaller time step is needed, Fig. 8.

The model results with the above space and time discretization are plotted for various time instants until the steady state in Fig. 9, and compared well with the corresponding analytical solutions. Finally, Fig. 10 shows the particles position and

velocity at two instant frames, one during the transient phase and the other during the steady state flow. From these two frames it can be observed that during the transient phase the influence from the movement of the upper plate has not yet reached the fluid particles that are closer to the lower one, while during the steady state the horizontal velocity of all the particles has evolved and reached its final linear profile.

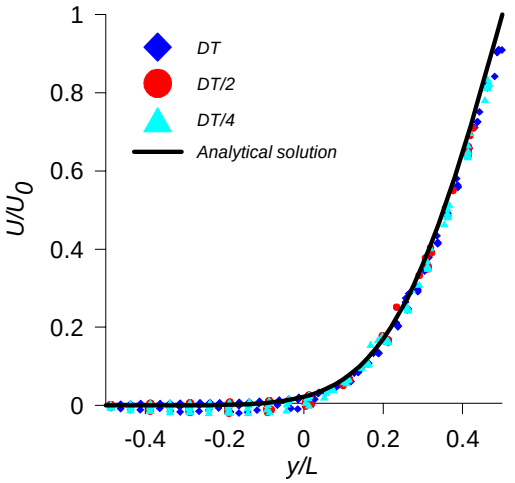

Figure 8. Results comparison for time independency.

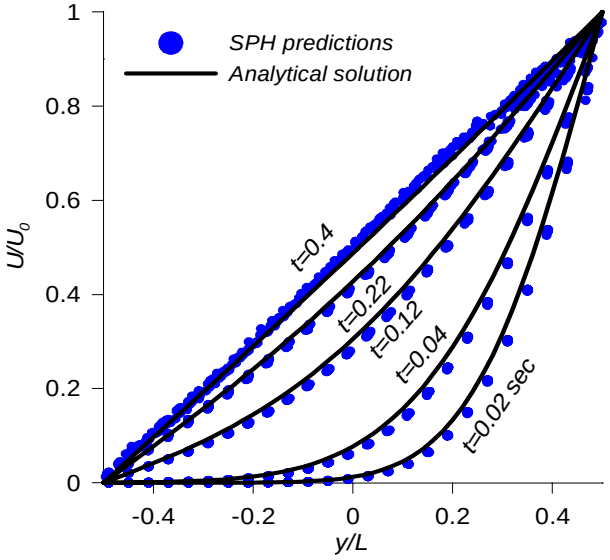

Figure 9. Comparative plots of velocity profiles at various time instants.

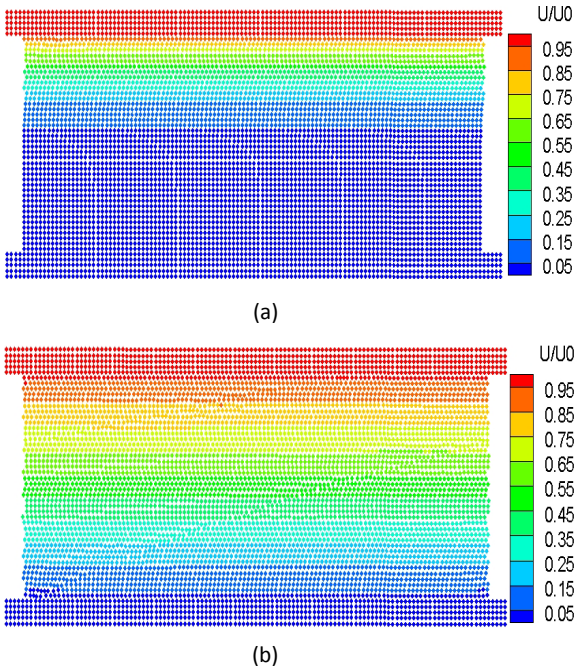

Figure 10. Frames for (a) Transient phase at t=0.02 sec. and (b) Steady state of the Couette Flow.

3.2 Poiseuille Flow

The second test case refers to the modelling of the 2D Poiseuille Flow. Once again the flow field is evolved between two infinite plates, which are located at $y=-L/2$ and $y=+L/2$, respectively (Fig. 11).

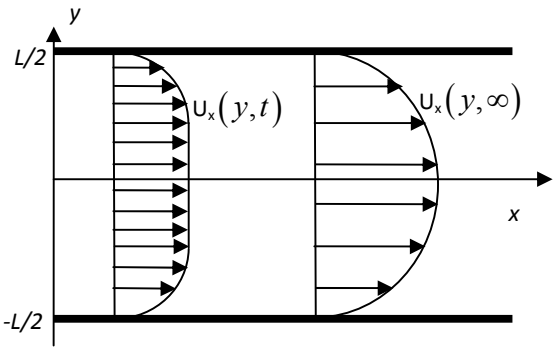

Figure 11. Poiseulle Flow

Initially for the simulation the system is at rest and at time $t=0$ a horizontal force F is exerted on the fluid particles, which sets them in motion. The flow field gradually evolves and finally reaches its steady state with a parabolic velocity distribution (Fig. 12).

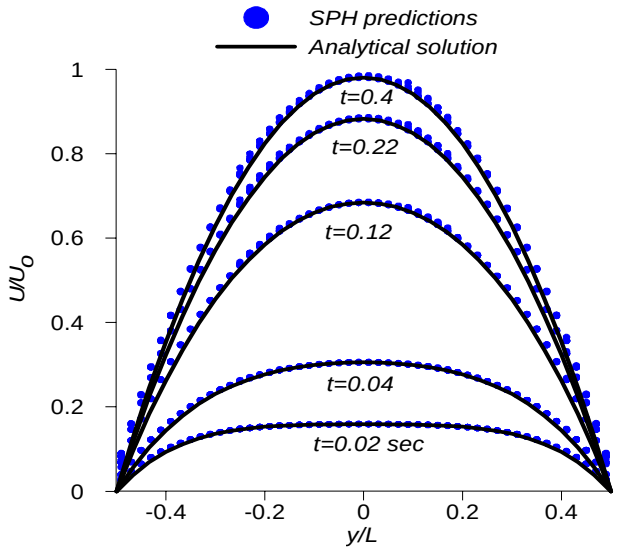

Figure 12. Results comparison for the velocity profiles at various time instants

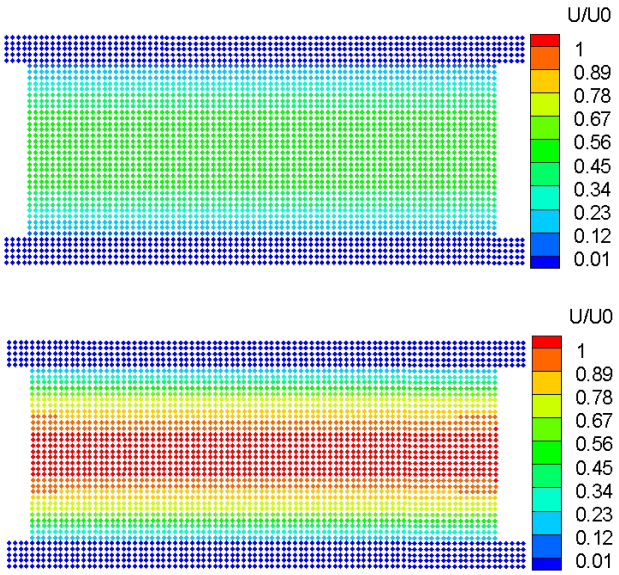

Figure 13. Transient phase and Steady state frames of the Poiseuille Flow.

The numerical results, which were obtained using the previous space and time resolution (L/50 and 6.25×10^{-4}) were tested against the analytical solution, which for the transient phase is expressed as follows [14]:

$$u_x(y,t) = \frac{F}{2\nu} y(y-L) + \sum_{n=0}^{\infty} \frac{4FL^2}{\nu\pi^3 (2n+1)^3} \sin\left(\frac{\pi y}{L}(2n+1)\right) \exp\left(-\frac{(2n+1)^2 \pi^2 \nu}{L^2} t\right) \quad (14)$$

where F is the horizontal force, which is calculated from the equation:

$$F = \frac{2\nu U_0}{(L/2)^2} \quad (15)$$

In the above equation U_0 is the peak fluid velocity at the steady state of the flow field evolution.

The comparison of the numerical results against the ones taken from the analytical solution is shown in Fig. 12, at various time instants. Once again the agreement of the results is very good and promising towards the use of the SPH method for the simulation of transient flow fields. Two instant frames showing the particles position and horizontal velocity during the transient phase and the steady state are shown in Figure 13.

In Fig. 13 it can be observed that during the transient phase the existence of the viscosity forces decelerates the velocity evolution of the particles, while during the steady state the velocity distribution has reached its final parabolic profile.

3.2 Dam break

The classical problem of Dam Break [17]-[18] is also used for the validation of the developed model. The test case refers to a water column, which is suddenly allowed to collapse into a rectangular tank (Fig. 14).

Figure 14. Setup of the Dam Break problem.

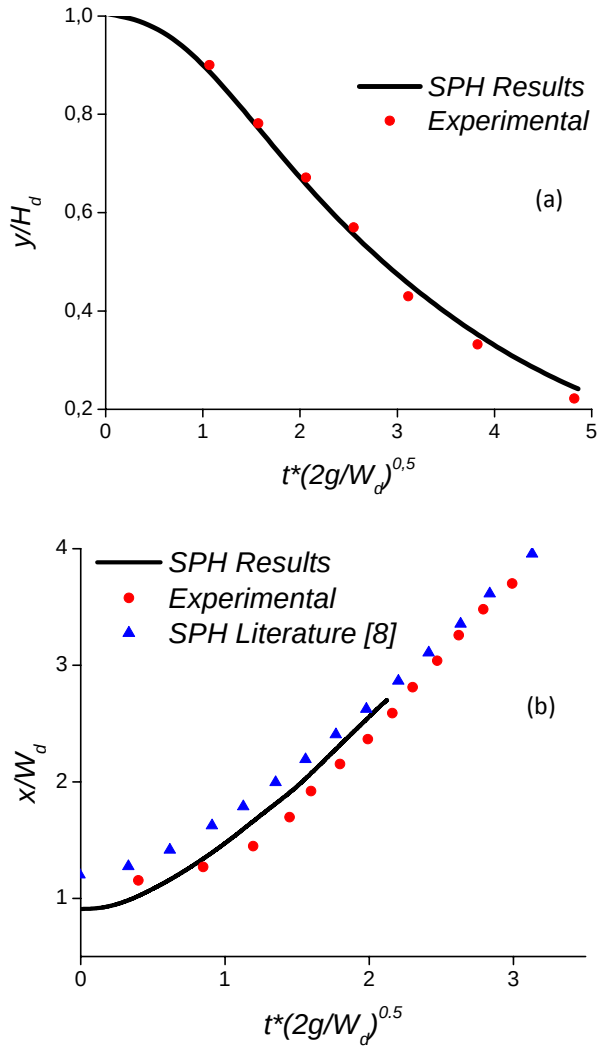

Figure 15. (a) Maximum column height and (b) position of the leading edge versus time.

The experimental data [17] for this test case contain the maximum height and the leading edge position of the collapsing column versus time. The SPH model results are compared with the measurements in Fig. 15, showing quite good agreement when referring to the decrease of the maximum height of the column. The deviation of the leading edge position curve from the experimental data , Fig. 15(b), is expected as from [8].

Finally, an important advantage of the SPH method is its ability to provide a good qualitative view of complex, unsteady two-phase flows in a fast and reliable way. Some indicative plots showing the evolution of the liquid column collapse are given in Fig. 16, for various non-dimensional time instants.

4 Conclusions

A gridless flow simulation algorithm based on the SPH method was developed and applied for the simulation of three test cases of 2D viscous incompressible flows. The numerical experiments confirmed at first the efficiency of the method in reproducing complex transient and multiphase flows. The capability of providing in a fast and robust way a detailed and reliable qualitative picture of the flow evolution, in an animation form, is valuable for the study and better understanding of such flows, and cannot be easily obtained by other continuous methods (Eulerian or Navier-Stokes). Also, the quantitative results were very encouraging showing that the method is trustworthy for further investigation in order to apply in complex practical flows encountered in impulse water turbines.

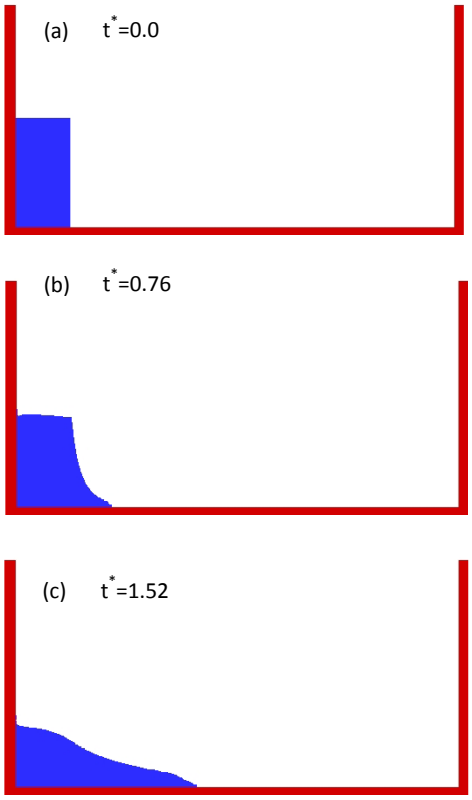

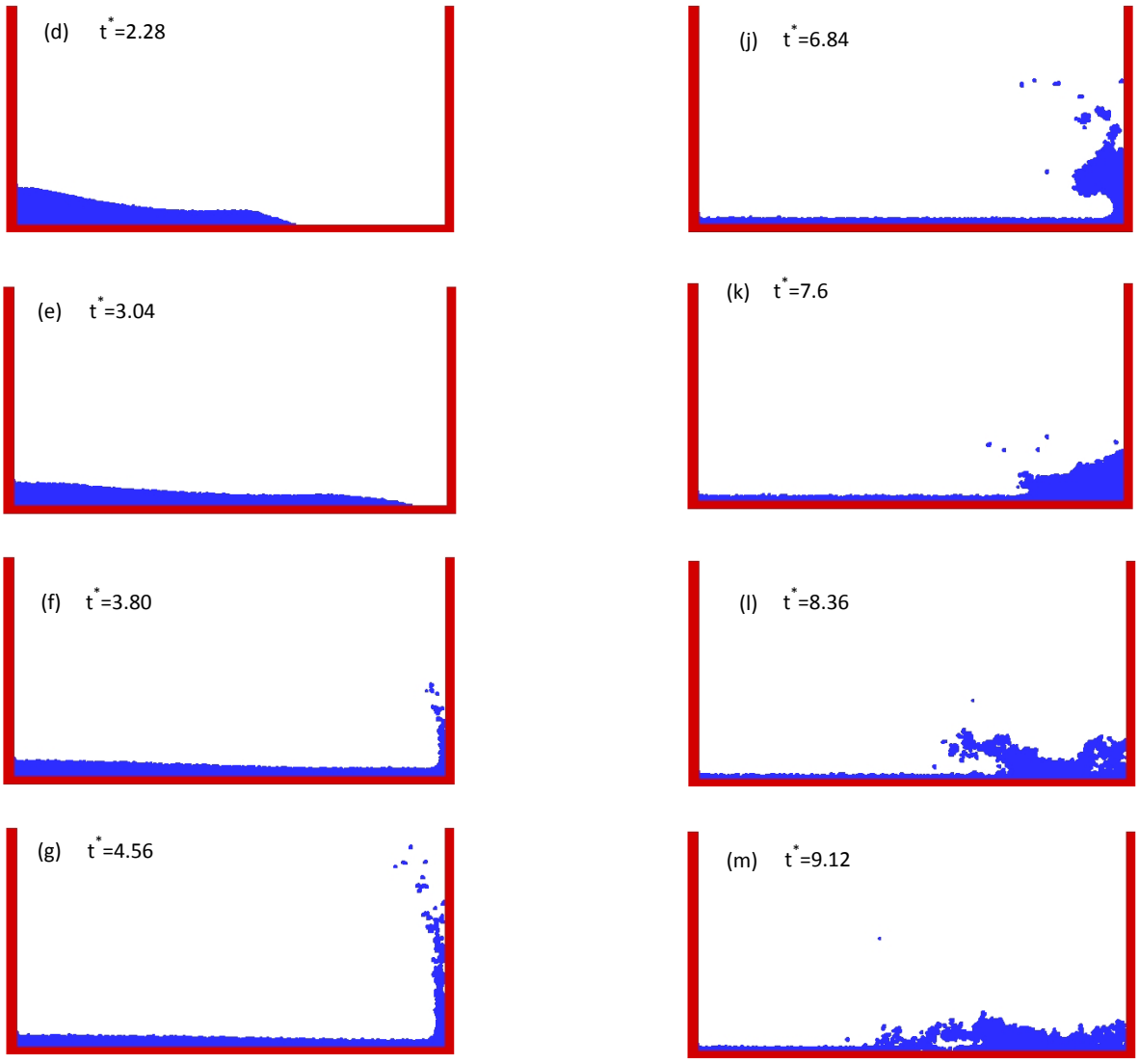

Figure 16. Instant frames of the collapsing water column, where $t^*=t(2g/W_d)^{0.5}$.

References:

1. Lucy, L.B., Numerical Approach to Testing of Fission Hypothesis. *Astronomical Journal*, Vol. **82**(12), 1977, pp. 1013-1024.
2. Gingold, R.A. and J.J. Monaghan, Smoothed Particle Hydrodynamics - Theory and Application to Non-Spherical Stars. *Monthly Notices of the Royal Astronomical Society*, Vol. **181**(2), 1977, pp. 375-389.

3. Monaghan, J.J., Smoothed particle hydrodynamics. *Reports on Progress in Physics*, Vol. **68**(8), 2005, pp. 1703-1759.
4. Monaghan, J.J., Simulating Free Surface Flows with SPH. *Journal of Computational Physics*, Vol. **110**(2), 1994, pp. 399-406.
5. Monaghan, J.J. and A. Kos, Solitary waves on a Cretan beach. *Journal of Waterway Port Coastal and Ocean Engineering-Asce*, Vol. **125**(3), 1999, pp. 145-154.
6. Liu, G.R., Smoothed Particle Hydrodynamics - A meshfree Particle Method. Vol. 2003.
7. Cleary, P., et al., Flow modelling in casting processes. *Applied Mathematical Modelling*, Vol. **26**(2), 2002, pp. 171-190.
8. Colagrossi, A. and M. Landrini, Numerical simulation of interfacial flows by smoothed particle hydrodynamics. *Journal of Computational Physics*, Vol. **191**(2), 2003, pp. 448-475.
9. Takeda, H., S.M. Miyama, and M. Sekiya, Numerical-Simulation of Viscous-Flow by Smoothed Particle Hydrodynamics. *Progress of Theoretical Physics*, Vol. **92**(5), 1994, pp. 939-960.
10. Dalrymple, R.A. and B.D. Rogers, Numerical modeling of water waves with the SPH method. *Coastal Engineering*, Vol. **53**(2-3), 2006, pp. 141-147.
11. Monaghan, J.J. and J.C. Lattanzio, A Refined Particle Method for Astrophysical Problems. *Astronomy and Astrophysics*, Vol. **149**(1), 1985, pp. 135-143.
12. Morris, J.P., A study of the stability properties of smooth particle hydrodynamics. *Publications Astronomical Society of Australia*, Vol. **13**(1), 1996, pp. 97-102.
13. Violeau, D. and R. Issa, Numerical modelling of complex turbulent free-surface flows with the SPH method: an overview. *International Journal for Numerical Methods in Fluids*, Vol. **53**(2), 2007, pp. 277-304.
14. Morris, J.P., P.J. Fox, and Y. Zhu, Modeling Low Reynolds Number Incompressible Flows Using SPH. *Journal of Computational Physics*, Vol. **136**(1), 1997, pp. 214-226.
15. Oger, G., et al., Two-dimensional SPH simulations of wedge water entries. *Journal of Computational Physics*, Vol. **213**(2), 2006, pp. 803-822.
16. Jiang, F., M.S.A. Oliveira, and A.C.M. Sousa, SPH simulation of low Reynolds number planar shear flow and heat convection. *Materialwissenschaft Und Werkstofftechnik*, Vol. **36**(10), 2005, pp. 613-619.
17. Ubbink, O., Numerical prediction of two fluid systems with sharp interfaces. Vol. 1997.
18. Bonet, J. and T.S.L. Lok, Variational and momentum preservation aspects of Smooth Particle Hydrodynamic formulations. *Computer Methods in Applied Mechanics and Engineering*, Vol. **180**(1-2), 1999, pp. 97-115.